

# Minimal mechanism for flocking in phoretically interacting active colloids

Arvin Gopal Subramaniam,<sup>1,2,\*</sup> Sagarika Adhikary,<sup>1,2,†</sup> and Rajesh Singh<sup>1,2,‡</sup>

<sup>1</sup>*Department of Physics, Indian Institute of Technology Madras, Chennai 600036, India*

<sup>2</sup>*Center for Soft and Biological Matter, IIT Madras, Chennai 600036, India*

Collective motion as a flock is a widely observed phenomenon in active matter systems. We report a novel flocking transition mechanism in a system of chemically interacting active colloidal particles sustained purely by chemo-repulsive torques at low to medium densities. The basic requirements to maintain the polar liquid flock are excluded volume repulsions and deterministic long-ranged net repulsive torques. The mechanism we report requires that the time scale individual colloids move a unit length to be dominant with respect to the time they deterministically sense chemicals. This can be equivalently interpreted as pair colloids sliding a minimal unit length before deterministically rotating due to chemical interactions. Switching on the translational repulsive forces renders the flock a crystalline structure. We complement these results with an analysis of a continuum hydrodynamic model, with the transition corresponding to destabilization of the flocking state. Finally, we present simulations for flocking in an agent-based model consisting of local update rules of colloidal pairs that slide and rotate upon collision.

## I. INTRODUCTION

The collective swarming behaviour of interacting agents - also called flocking [1] - has been a topic of sustained interest in the field of non-equilibrium statistical physics. Flocking is also a ubiquitous phenomena in the natural world, widely reported in groups of animals such as birds, fish, and mammals [2]. Paradigmatic models that incorporate short-ranged alignment interactions to study flocking have been extensively studied [1, 3–5] and continue to be investigated [6–10]. In the Vicsek model [3], local alignment interactions among the individual agents can lead to transition from a disordered state to one with large-scale, coordinated movement. The flocking transition in Vicsek-like models with short-range interactions has been widely studied, and traveling density bands are observed at the onset of transition [4, 5, 11, 12].

The possibility of attaining an emergent global polar order (flocking) arising purely out of dynamical particle-based models, without any explicit alignment interaction, is a subject of recent interest. Studies on these include those studying the interplay between non-equilibrium phase separation [13] and other collective dynamics [14–17], those that study the effect of velocity alignment interactions [18–20], models incorporating attractive interactions [21, 22], history-dependence [23, 24], and those that exclusively study the effect of repulsive forces and torques [25, 26]. Though various possible mechanisms deviating from the Vicsek-like phenomenology have been established, the explicit relevance of the separate force and torque contributions have not been established. For instance, migrating cells that display a global polarity have been known to display chemo-tactic attractive interactions in addition to (among others) either a contact “inhibited” or “attracted” locomotion - akin to a

long-ranged torque of either repulsive or attractive nature [22, 27, 28]. Thus, open questions remain on the minimal ingredients and mechanism at play arising from the rotational and translational components separately.

In this paper, we report a novel flocking mechanism for polar liquids where colliding pair particles have to sufficiently slowly rotate in response to chemical gradients before moving a unit distance upon collision. The basic ingredients that are *sufficient* to produce such a flock are thus (i) short-ranged excluded volume repulsion, and (ii) long-ranged (chemo) repulsive torques. There is no need for any additional (chemo)repulsive translational forces between the particles, nor is there a requisite role for noise in destabilizing the flock. The incorporation of long-ranged translational chemo-repulsive forces between the particles induces instead a crystalline flock (with regular lattice spacing). We demonstrate that the flocking persists even for a chemo-attractive translational force.

The remainder of the paper is organized as follows. In section II, we describe our model to study phoretic interactions of active particles. Our main results are given in section III. In this section, we report our results from particle-based numerical simulations by mapping phase diagrams and describe the properties of the distinct flocking states. Then, we complement the results from particle-based simulation with an analysis of a continuum description in section IV. To make sense of these results further, in section V, we construct an agent-based “sliding model”, where the only interactions are pair colloids that slide and rotate upon contact with each other. Finally, we conclude in section VI by summarizing our main results and comparing it with existing literature, along with suggesting directions for future investigations. In what follows, we describe our model and detail our results.

\* Contributed equally; ph22d800@smail.iitm.ac.in

† Contributed equally; a.sagarika@physics.iitm.ac.in

‡ rsingh@physics.iitm.ac.in

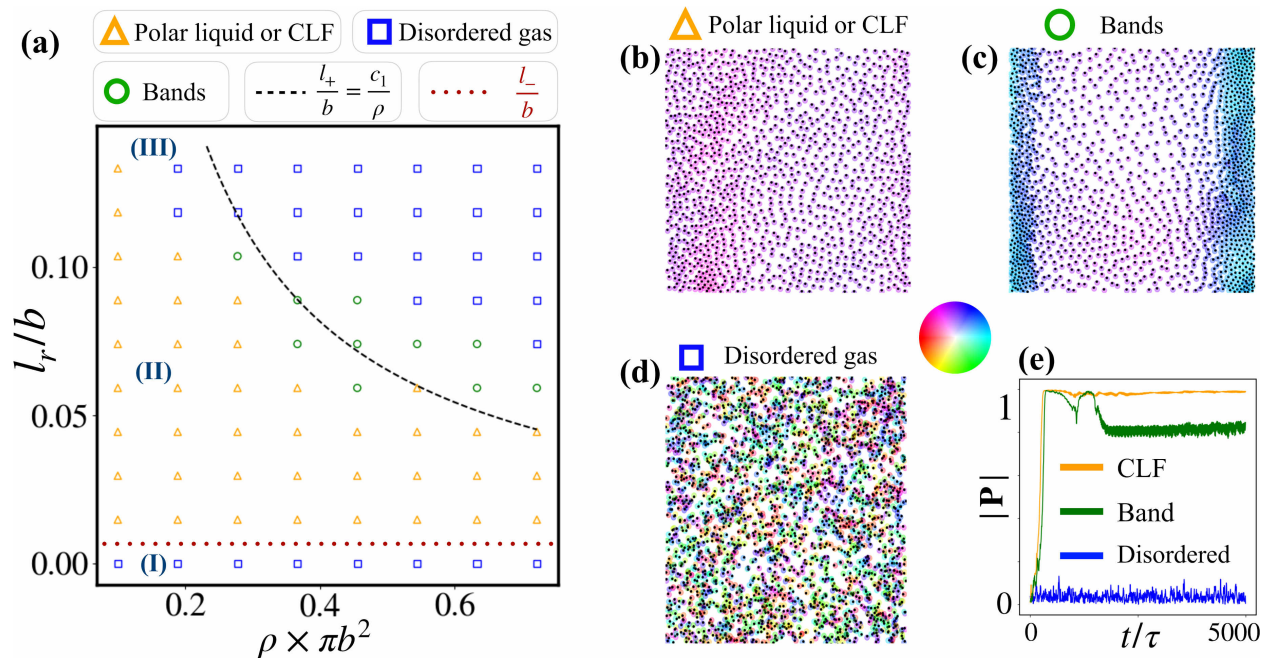


FIG. 1. Polar liquid flocks for  $\chi_t = 0$ . (a) Phase diagram in the  $(\rho, l_r/b)$  plane. Symbols here and throughout the paper denoting a flock (yellow triangle), bands (green circles), and disordered (blue squares). Marked (I)-(III) scenario and transition lines (black and red) are described in the schematic shown in Fig. 2. Snapshots of the respective phases are shown in (b)-(d) respectively (color coding for orientation of each particle is in middle panel). (e) The evolution of the polarization is displayed for the corresponding states (similarly colored). See Movie I [29] for dynamics to obtain CLF starting with a disordered state.

## II. MODEL

We consider a set of  $N$  chemically interacting polar colloids, where chemical is assumed to be instantaneously deposited on the colloidal surfaces [30–33]. We model the  $i$ th active particle as a colloid particle centered at  $\mathbf{r}_i = (x_i, y_i)$ , confined to move in two-dimensions, which self-propels with a speed  $v_s$ , along the directions  $\mathbf{e}_i = (\cos \theta_i, \sin \theta_i)$ . Here  $i = 1, 2, 3, \dots, N$  and  $\theta_i$  is the angle made by the orientation  $\mathbf{e}_i$  with respect to the positive  $x$ -axis. The orientation  $\mathbf{e}_i$  of the  $i$ th particle, given in terms of the angle  $\theta_i$ , changes due to coupling its dynamics to the dynamics of a phoretic (scalar) field  $c$ , as we describe below. The position  $\mathbf{r}_i$  and orientation  $\mathbf{e}_i$  of the  $i$ th particle is updated as:

$$\dot{\mathbf{r}}_i = \mathbf{V}_i, \quad \mathbf{V}_i = v_s \mathbf{e}_i + \chi_t \mathbf{J}_i + \mu \mathbf{F}_i + \boldsymbol{\eta}_i^t, \quad (1a)$$

$$\dot{\mathbf{e}}_i = \boldsymbol{\Omega}_i \times \mathbf{e}_i, \quad \boldsymbol{\Omega}_i = \chi_r (\mathbf{e}_i \times \mathbf{J}_i) + \boldsymbol{\eta}_i^r. \quad (1b)$$

For full generality, Eq. (1) is written with both translational and rotational terms, the respective chemical susceptibilities are denoted  $\chi_t$  and  $\chi_r$  respectively. Here,  $\boldsymbol{\eta}_i^t$  and  $\boldsymbol{\eta}_i^r$  are white noises with zero mean and no temporal correlation. The variance of noises  $\boldsymbol{\eta}_i^t$  and  $\boldsymbol{\eta}_i^r$ , are respectively,  $2D_t$  and  $2D_r$ . These noises terms are included for the sake of completion and to demonstrate that our results are robust against weak fluctuations. In this paper, the fluctuations are set to be negligibly small to emphasize that flocks can be formed and destroyed by deterministic causes [34].

The inter-particle interaction (of chemical origin) is given in terms of the phoretic current:  $\mathbf{J}_i(t) = -[\nabla c(\mathbf{r}, t)]_{\mathbf{r}=\mathbf{r}_i}$ , where  $c(\mathbf{r}, t)$  is the concentration of the chemicals (e.g filled micelles in an oil-emulsion system [23, 35]). The concentration field evolves in time as:

$$D_c \nabla^2 c(\mathbf{r}, t) + \sum_{i=1}^N c_0 \delta(\mathbf{r} - \mathbf{r}_i) = 0. \quad (2)$$

Here,  $D_c$  is the diffusion coefficient and  $c_0$  is emission constant of the chemical. The solution of the above can be used to compute  $\mathbf{J}_i$  as:

$$\mathbf{J}_i = \frac{c_0}{4\pi D_c} \sum_{\substack{j=1 \\ i \neq j}}^N \frac{\mathbf{r}_{ij}}{r_{ij}^3} \quad (3)$$

Here,  $r_{ij} = |\mathbf{r}_{ij}|$ , with  $\mathbf{r}_{ij} = \mathbf{r}_i - \mathbf{r}_j$ . The term proportional to  $\chi_r$  in Eq.(1) drives orientational changes (turning away from each other if  $\chi_r > 0$ ) through interparticle chemical interactions. In this paper, we only consider case of  $\chi_r > 0$  when particles turn away from each other due to chemical interactions [23, 24]. Similarly, the term proportional to  $\chi_t$  ensures repulsion in the positional dynamics if  $\chi_t > 0$ . Here, both  $\chi_r$  and  $\chi_t$  are positive (unless otherwise stated) and the system is said to be *chemo-repulsive*. To preclude overlap of the particles, there is a force on the particles:  $\mathbf{F}_i = -\nabla_i \mathcal{U}$ , while,  $\mathcal{U} = \sum_{i < j} \mathcal{U}^e(\mathbf{r}_i, \mathbf{r}_j)$ . With  $b$  as the colloidal radius, we choose  $\mathcal{U}^e$  to be of the form:  $\mathcal{U}^e = \kappa (r_{ij} - 2b)^2$

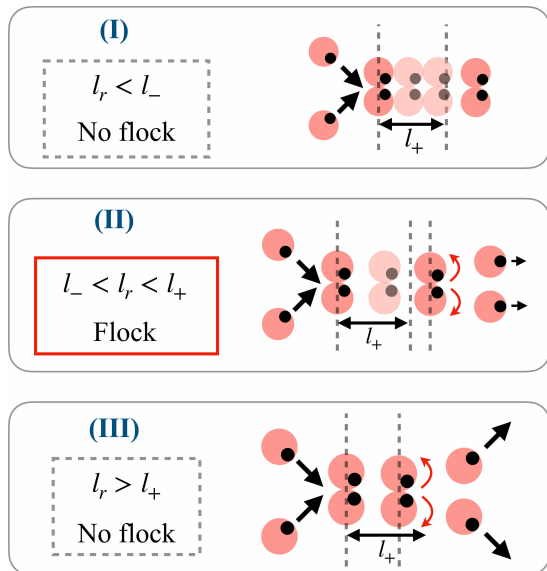


FIG. 2. Schematic of the mechanism for formation of fluid flocks. *Top-to-bottom*: Series of scenarios depicted corresponding to parameters choices labelled in Fig. 1a.  $l_-/b$  is annotated as a dotted red line in (a), while the density dependent  $l_+/b$  in dashed black line. The middle panel (II) shows the pair collision mechanism that would produce a flock; this occurs is the chemical sensing occurs after sliding a length  $l_{sl}^+$ . Top (I) and bottom (III) panels show scenarios where the chemical response is either too quick or too slow, such that a stable flock cannot be formed

if  $\tau_{ij} < 2b$ , while it vanishes otherwise. Here,  $\kappa$  is a constant. Simulation details along with the full set of parameters used to generate each figure is given in the Appendix A.

### III. RESULTS

We first summarize our main results for the case of  $\chi_t = 0$  (no chemorepulsive forces between the particles). In particular, we report here polar fluids that are obtained due to chemo-repulsive torques alone ( $\chi_r > 0$ ). See Fig. 1. These flocks are obtained only if pair colloids move at least a distance ( $l_{sl}^+$ , defined later) before deterministically rotating away due to sensing of chemical gradients. The schematic of the mechanism for polar fluids that we report is presented in Fig. 2. For  $\chi_t > 0$ , we obtain crystalline flocks that are obtained via a combination of repulsive torques and forces (Fig. 3(c)); we also find these crystals for (a narrow range of) *attractive* forces (Fig. 3(b)). For the rest of the paper we denote the former as ‘‘Chemorepulsive Liquid Flocks’’ (CLF), and the later as ‘‘Chemorepulsive Crystalline Flocks’’ (CCF).

#### A. CLFs via long-ranged repulsive torques

We first consider the case of  $\chi_t = 0$ , thus repulsions are only short-ranged that avoid overlap of the particles in the system via  $\mathbf{F}_i$ . The phase diagram delimiting polar flocks (or CLF), bands, and disordered states are shown in Figure 1(a). The states are delimited via the mean global polarization of the system at the steady state,  $\langle |\mathbf{P}| \rangle_{ss}$ , where  $\mathbf{P} = \frac{1}{N} \sum_{i=1}^N \frac{\mathbf{e}_i}{|\mathbf{e}_i|}$ . On the  $(\rho, \chi_r)$  plane (Fig. 1(a)), we see that low density flocks are sustained, that are eventually destabilized at sufficiently high repulsion and densities. These flocks have evidently a liquid-like spatial structure (Fig. 1(b); see also Fig. 3(d)) [25, 36, 37]. The density field  $\rho$  is thus not homogeneous across the system (see Fig. 1(c); (see also Appendix B)). We note that  $\tau = b/v_s$  is the propulsion time scale. In addition, we define  $\tau_f = b^3/\chi_r$ , which sets the time scale for deterministic rotation of the particle due to phoretic interactions.

The phenomenology of the CLF can also be understood by a comparison of the relevant length scales of the problem. First, we write down natural length scales that arise out of the equations of motion (1). They are:

$$l_r = \frac{\chi_r}{bv_s}, \quad l_t = \frac{\chi_t}{b^2v_s}. \quad (4)$$

They are, respectively, the deterministic rotation and translational lengths; these quantify the length scales within the system where colloids instantaneously sense long-ranged chemical gradients for the rotational and translational dynamics respectively. From the phase diagram, we see that there are separate length scales that arise as a consequence of the collective many-body dynamics.

To make sense of the above phenomenology, let us construct a *sliding* time (length) scale, which represents the typical time (length) pair colloids would co-move upon collision before rotating away. The sliding time  $\tau_{sl}$ , given by  $\tau_{sl} = \frac{b^2}{v_s \tau_r}$ .  $\tau_{sl}$  is time during which pair colloids slide a distance  $l_{sl} = v_s \tau_{sl} = \frac{v_s b^3}{\chi_r}$  whilst rotating. Let us denote  $l_-$  as the smallest length to sustain the CLF (corresponding to the lowest transition line), and  $l_+$  as the (density dependent) length scale above which the CLF is not sustained. The mechanism for the CLF can then be understood as a competition between  $l_r$  and  $l_+$ ,  $l_-$ ; this is illustrated in Fig. 2 (annotated accordingly in the phase diagram of 1(a)). In the moderate density region, we consider a series of transitions from disorder-to-order-to-disordered phases. When  $l_r < l_-$  (corresponding to  $l_{sl} > l_{sl}^-$ ) (*bottom*), we have a *sub-deterministic* sensing of the chemicals; here the orientational changes of the colloids are too slow compared to the free movement time, pair colloids slide excessively long, hence local polar order cannot be sustained. Increasing  $l_r$ , in the regime of  $l_- < l_r < l_+$  (equivalently  $l_{sl}^+ < l_{sl} < l_{sl}^-$ ) (*middle*), we have that the chemical response time fast enough such that local polar order is sustained, but still sufficiently

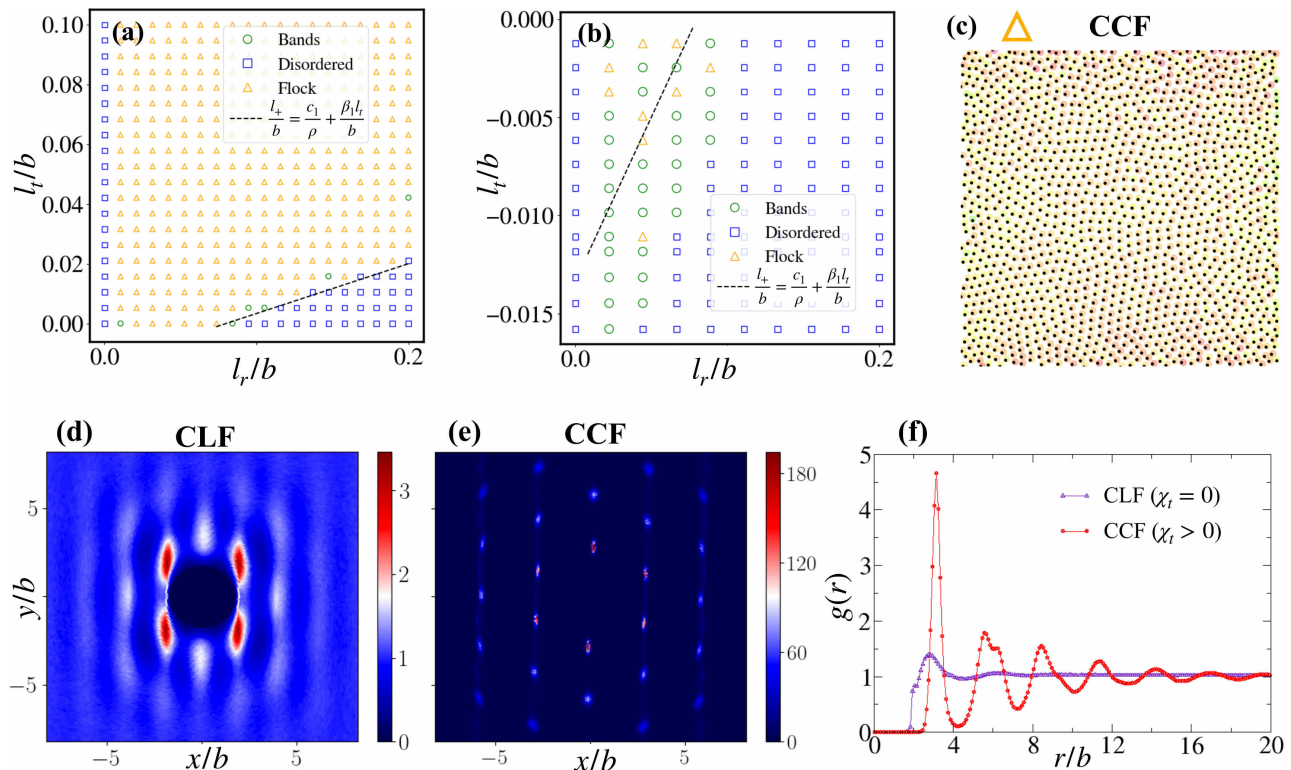


FIG. 3. (a) Phase diagram in the  $(l_r/b, l_t/b)$  plane for the case of  $\chi_t > 0$ . Dashed line refers to lower bound on  $\chi_r$ , solid line for lower bound on  $\chi_r$  from (5). (b) Similar phase diagram for the case of  $\chi_t < 0$  (extension of (a)). The transition line is extrapolated from (3)(a). (c) Shows a snapshot of the CCF phase (same color scheme as in Fig (1)). See Movie II [29] for dynamics to obtain CCF starting with a disordered state. (d) and (e) compare  $g(r, \phi)$  for the case of the CLF and the CCF. Corresponding (f) Pair correlation  $g(r)$  plot, in the flocking phase, for CLF and CCF.

slow to break forward-backward symmetry at the pair collision level. Finally for  $l_r > l_+$  (equivalently  $l_{sl} < l_{sl}^+$ ), the chemical response is sufficiently quick such that there is no symmetry breaking at the pair collision level. We note that from simulations at  $\rho \approx 0.1$  these values we find to be  $l_{sl}^+ \sim 8.3b$  and  $l_{sl}^- \sim 100b$ . We conclude that a pair of colloids have to slide at least a distance  $l_{sl}^+$ , before deterministically turning away, as the underlying mechanism for the CLF.

### B. Effect of long-ranged translational repulsion

We now switch on  $\chi_t$  and ask how the properties of the flock differ. On the  $(l_r/b, l_t/b)$  plane, we find that there is a clear region of flocking for non-zero  $\chi_t$  (see Figure 3(a)). We further find that the flocks have crystalline order (see Figure 3(c),(e)). Such crystalline flocks in repulsive systems have been recently reported [26]. Similarly to the CLF, the CCF destabilized by sufficiently high rotational torques. In addition,  $l_+$  now is linear in  $l_t$ .  $l_+$  being larger for a positive  $l_t$ , this thus renders a shorter sliding length for pair colloids during the CCF formation. The net result is thus a shorter sliding length compared to the CLF, which we can attribute to the difference be-

tween crystalline and liquid structures. We note that if this repulsion is too strong, the CCF is destabilized to a disordered gas (not shown here). The most generic form of the transition lines from the phase diagrams can be written as

$$l_r < l_+, \quad \frac{l_+}{b} = \frac{c_1}{\rho} + \frac{\beta_1 l_t}{b} \quad (5)$$

which is presented in Figures (1)(a) and (3)(a). We obtain  $\beta_1$  and  $c_1$  by first fitting the boundary line in Fig. 3(a). The slope gives  $\beta_1 \approx 0.167$ , whilst the  $x$ -intercept gives  $c_1 \approx 0.104$ . This  $c_1$  then independently fixes the boundary on Fig. 1(a). We show below how this can be derived from a continuum model of interacting density and polarization fields. The  $\frac{c_1}{\rho}$  term promotes sliding at high densities. This effect can be understood by comparing  $l_{sl}$  with the mean free path  $l_\rho = \frac{1}{\sqrt{\rho}}$ . At density values higher than  $\rho_c = (bc_1)^{2/3} \approx 0.058$  we have that  $l_{sl}$  exceeds  $l_\rho$ . Thus, for  $\rho > \rho_c$ , sliding is exaggerated via a confinement of pair colloids due to frequent collisions. If excessive, this effect can bring  $l_{sl}$  close to the upper bound  $l_{sl}^-$ , inhibiting flock formation at high densities. Instead for  $\rho < \rho_c$ , this effect is suppressed, and the pair sliding mechanism happens uninhibited, encouraging flock formation. Both these effects are consistent

with our results in Fig. 1(a). This thus restricts the density range within which fluid flocks can form. For  $\chi_t > 0$ , the second term further suppresses the sliding length due to long-ranged translational repulsion. Sliding over shorter distances effectively localizes particles in space and the effect is a crystalline structure.

We note that the flock destabilization mechanism here is independent of the contribution of noise. Though we have explicit noise terms in the updates in Eq.(1) for the sake of completion, they are set to be negligibly small (see Table I in Appendix). Indeed, if we were to define length scales  $l_\eta = \frac{D_r b^2}{v_s}$  and  $l_\xi = \frac{D_t}{v_s}$ , using the values used of  $D_r \approx 10^{-6}$  and  $D_t \approx 10^{-8}$ , we find that  $l_\eta \sim 10^{-4}b$  and  $l_\xi \sim 10^{-6}b$ , thus negligible compared to all other length scales in the problem. We have repeated all the simulations presented in Fig. (1) with  $D_r = D_t = 0$ , and have found the results to be identical. Thus, as opposed to the conventional picture of noise induced inhibition of flock formation [4, 11, 21, 26] (i.e. deterministic alignment interactions compete with randomness in the same interaction channel), our mechanism reports a competition between a *deterministic* length scale due to sensing of chemical gradients  $l_r$  (also  $l_t$ ) and other deterministic length scales of the problem.

### C. Difference between CCF and CLF

The difference in spatial structure between the CLF and CCF is readily distinguished by the pair correlation function  $g(r) = \frac{1}{N} \sum_{i,j} \delta(r - |\mathbf{r}_i - \mathbf{r}_j|)$ . This is plotted in Fig. (3)(f), distinguishing the solid and liquid signatures [25]. A closely related quantity [38] is the polar pair correlation  $g(r, \phi)$  which explicitly depends on the orientations of the colloids. Here,  $\cos(\phi_{ij}) = \mathbf{e}_i \cdot (\hat{r}_i - \hat{r}_j)$ [38]. For the CLF, we see that there are quadrants where neighbours are more likely to be found (3(d)), as opposed to the hexatic order of the CCF (3(e)). In the case of CCF, the intensity (proportional to the probability of finding the particle from the reference - see Appendix B) in the well-localized hexagonal positions of the crystal are substantially higher than in the CLF, which are instead less intense with a greater relative spread. The quadrant-like distribution indicate the repulsive torque-induced turn away of the particles in the forward and backward direction of the reference particle.

An additional feature of the CLF is that they have a steady-state persistent fluctuations of both density and polarization fields (dynamical steady-state - note that our simulations are effectively noiseless), which is absent in the CCF (see appendix B and Fig. 8). Further, we note that both the CCF and CLF show an enhanced number fluctuations  $\langle (\Delta N)^2 \rangle \sim N^\alpha$  with  $\alpha \sim 1.2$  [1, 39, 40].

To further support the robustness of the mechanism we report CLFs arising repulsive torques with the addition of long-ranged *attractive* interactions, thus  $\chi_t < 0$ . We find that this phenomenology is maintained for  $l_t \in [0, -0.01]$ ,

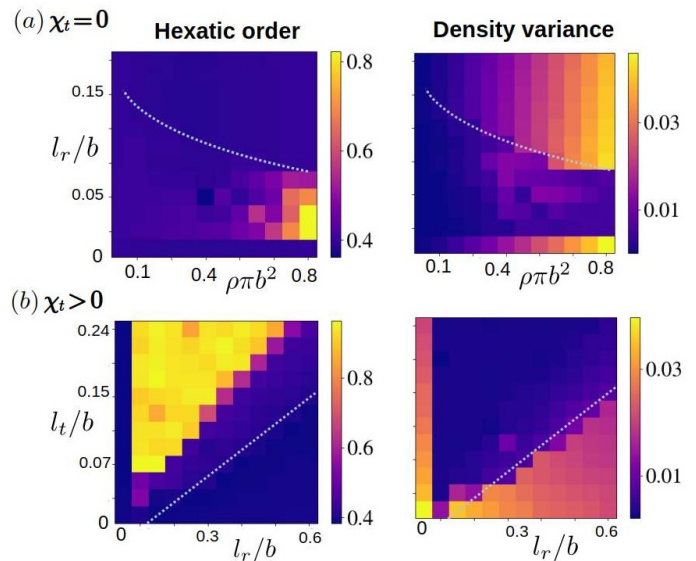


FIG. 4. Phase diagrams in terms of (left) global hexatic order ( $\psi_6$ ) and (right) density variance. The panel on *top* shows results for the case (a), which is  $\chi_t = 0$ , whereas the *bottom* panel shows results for the case (b), which is  $\chi_t > 0$ . Dotted curves indicate flocking order-disorder transition line. See text for details.

before transitioning to a disordered gas for larger attractive translational interactions; this is shown in Figure 3(b). Putatively, the clumping tendency in this range is balanced by the excluded volume repulsions.

### D. Hexatic order and Density variance

One defines a measure of local hexatic order  $\psi_i$  for the  $i$ th particle to quantify the hexatic order globally in terms of  $\psi_6$ . They are given as [41]:

$$\psi_6 = \frac{1}{N} \sum_i \psi_i, \quad \psi_i = \frac{1}{N_i^n} \sum_j e^{i6\theta_{ij}}. \quad (6)$$

Here,  $\theta_{ij}$  is the angle between particle  $i$  and particle  $j$ , and  $N_i^n$  is the number of neighbors for particle  $i$  ( $N^n \approx 6$  for all data points). The observable  $\psi_6$  is then averaged over 1000 different particle configurations at the steady-state. We plot  $\psi_6$  for the two cases ( $\chi_t = 0$  and  $\chi_t > 0$ ) in the left panel of Fig. 4. The transition lines from the phase diagrams in Figures 1(a) and 3(a) are also shown as dotted lines for guide to the eye. In the case of  $\chi_t = 0$  (Fig. 4(a) left), the hexatic order exists in the flocking phase, only for a very high density (area fraction  $\rho\pi b^2 > 0.6$ ). Whereas, in case of  $\chi_t > 0$  (Fig. 4(b) left), with  $\rho\pi b^2 = 0.36$ , the system becomes highly hexatic in the flocking phase. However, near the transition line, where density bands are prone to occur, the hexatic order gradually decreases.

Next, density variance for the two cases ( $\chi_t = 0$  and  $\chi_t > 0$ ) are shown in the right panel of Fig. 4. The density variance [15] is calculated from the density distribution for a specific parameter set shown in the phase diagram. For local density measurements, the Voronoi tessellation method has been implemented for a spatial configuration of particles. We calculate local density  $\rho_l = \frac{\pi b^2}{A_l}$ , where  $A_l$  is local area assigned to each particle. Then we compute the density variance as  $\langle \rho_l^2 \rangle - \langle \rho_l \rangle^2$  (spatial average) and finally averaged over 1000 configurations. In both cases, the density variance is much lower in the flocking state. However, it shows an increase near the transition region. The density variance is high for the high area fraction ( $\rho\pi b^2$ ) and in the disordered phase, for the case  $\chi_t = 0$  (Fig. 4(a) right panel). For  $\chi_t > 0$  case, with low  $\chi_t$  values, the variance is more prominent, shown in Fig. 4(b) (right panel).

### E. CCFs as solutions to equation of motion

Our choice of EOM in (1) is also unique in that it can be shown to support crystalline flocks as its dynamical fixed points. To see this, we firstly note that from the EOM the fixed points of  $\theta_i$  are obtained by setting  $\Omega_i = 0$ , giving

$$\theta_i^* = \tan^{-1} \left( \frac{\sum_{j \neq i} (y_i - y_j) \prod_{k \neq i, j} |r_i - r_k|^3}{\sum_{j \neq i} (x_i - x_j) \prod_{k \neq i, j} |r_i - r_k|^3} \right) \quad (7)$$

The hexagonal structure of CCF makes (7) tractable. Firstly, let us consider a hexagonal lattice topology of distance  $2b'$  aligned along the direction of the flock  $\theta_i$  for the  $i$ th reference particle. To compute the sums in (7) one needs to evaluate the sums

$$\sum_j r_i - r_j = -b' \sum_{k=0}^K \sum_{n=1}^6 (1+k) \begin{pmatrix} \cos \left( (n-1) \frac{\pi}{3} - \theta_i \right) \\ \sin \left( (n-1) \frac{\pi}{3} - \theta_i \right) \end{pmatrix} \quad (8)$$

where  $K$  is the upper bound on the radial sums performed on the lattice; in our case  $K = \frac{50}{b} - 1$ . To evaluate  $\prod_{k \neq i, j} |r_i - r_k|^3$ . We can evaluate this to be  $\prod_k^K ((1+k)b')^{z-1} \delta_{k, j \in \{k\}} ((1+k)b')^z (1 - \delta_{k, j \in \{k\}})$ , thus raised to power coordination number  $z$  minus one for the radial coordinate containing the  $j$ th particle (denoted by  $j \in \{k\}$ ), and to the coordination number for all other radial coordinates. We recognize immediately that the symmetry of the lattice structure means that this depends on only the location of the ‘‘left out’’ particle  $j$  and the reference particle  $i$ . Without loss of generality, we label this product  $P_{ij}$ . The sums over  $n$  for each component in (8) can be readily computed by applying the double angle formulae and symmetries of the sine and

cosine. The overall result is thus

$$\sum_j r_i - r_j = -b' \begin{pmatrix} \cos(\theta_i) \\ \sin(\theta_i) \end{pmatrix} S_K \quad (9)$$

where we have defined  $S_K = \sum_{k=0}^K (1+k)$  (not needed to be evaluated explicitly). Thus the fixed point angle of (7) simply reads

$$\theta_i^* = \tan^{-1} \left( \frac{\sum_j (y_i - y_j) P_{ij}}{\sum_j (x_i - x_j) P_{ij}} \right) \quad (10)$$

which we see to be the self-consistent  $\theta_i^* = \theta_i$  as required. Further, taking ratio of the coordinates of the positional dynamics at the fixed point, we see that  $\frac{y_i}{x_i} = \tan(\theta_i)$  as required. We thus conclude that our particular choice of chemical interactions of (3) supports a crystalline flock. For fluid flocks the result is less trivial since various sums and products need to be weighted by a distribution function. We nevertheless see that enhanced fluctuations of  $\theta_i^*$  is to be expected, since any approximate evaluation of (7) will contain various moments of each components of (8).

## IV. CONTINUUM DESCRIPTION

We write down here the coarse-grained hydrodynamic equations for the density  $\rho(\mathbf{r}, t)$  and polarization  $\mathbf{p}(\mathbf{r}, t)$  fields. The procedure is well established [38], and we can quote directly the equations:

$$\begin{aligned} \partial_t \rho &= -\nabla \cdot (v_{\text{tr}}(\rho) \mathbf{p} - D_{\text{tr}}(\rho) \nabla \rho) \\ \partial_t \mathbf{p} &= \Lambda(\rho) \frac{\nabla \rho}{2} + \frac{D_{\text{tr}}[\rho]}{\rho} [\nabla \cdot (\mathbf{p} \nabla \rho)] - D_r \mathbf{p} + D_t \nabla^2 \mathbf{p} \end{aligned} \quad (11)$$

Here, we have defined:

$$v_{\text{tr}} = v_s - \chi_t \xi_0 \rho, \quad D_{\text{tr}} = \xi_t \rho \chi_t, \quad \Lambda = \xi_r \chi_r \rho - v_{\text{tr}} \rho$$

where the constants  $\xi_0$ ,  $\xi_t$ , and  $\xi_r$  are obtained by fitting the continuum model to the transition line predicted by the particle-based simulation in Fig.1. From here on we set  $D_r$ ,  $D_t$  terms to zero in (12a) as they are negligibly small as explained in the previous section. In effect, the presence of these terms merely necessitate the formal coarse-graining procedure, but do not play any further role in explaining the instability of the flock.

We wish to study the flocking state, thus we linearize (12a) about the steady-state density and polarizations  $(\rho^*, \mathbf{p}^*)$ , defining  $(\delta\rho, \delta\mathbf{p}) = (\rho - \rho^*, \mathbf{p} - \mathbf{p}^*)$ . We use the following choice of Fourier basis expansion

$$\delta\tilde{\rho}(\mathbf{q}, \omega) = \int e^{i\mathbf{q}\cdot\mathbf{r}} e^{i\omega t} \delta\rho(\mathbf{r}, t) d^2\mathbf{r} \quad (12a)$$

$$\delta\tilde{\theta}(\mathbf{q}, \omega) = \int e^{i\mathbf{q}\cdot\mathbf{r}} e^{i\omega t} (\nabla \cdot \delta\mathbf{p}) d^2\mathbf{r} \quad (12b)$$

At the flocking state  $(\rho^*, \mathbf{p}^*)$  the following conditions hold:  $\nabla \rho^* \rightarrow 0$  and  $\nabla \cdot \mathbf{p}^* \rightarrow 0$ . We now consider cases of  $\chi_t = 0$  and  $\chi_t > 0$  separately.

### A. Case of $\chi_t = 0$

Here, we can solve equations (12a) in real space; we obtain an enslaved dynamics of  $\dot{\mathbf{p}}$  (instead of the conventional  $\mathbf{p}$ ) with respect to the density gradients:

$$\partial_t \mathbf{p} = \frac{\nabla \rho}{2} [(\chi_r \xi_r \rho - v_s)] \quad (13)$$

We see that for the temporal evolution of  $\mathbf{p}$  to be stable with respect to the density gradients (feedback response), we require the following:

$$\chi_r < \frac{v_s}{\xi_r \rho^*} \quad (14)$$

We see evidence for this enslavement in Fig. (1)(a). We see that the fluctuations in both  $\rho$  and  $\mathbf{p}$  are strongly coupled and that any fluctuations are stabilized in the long-time limit.

### B. General case with $\chi_t > 0$

Firstly, we may note that solving the  $\dot{\mathbf{p}} = 0$  in (12a) gives  $\rho^* = \frac{v_s}{\xi_r \chi_r + 2\xi_t \chi_t}$ , a generalization of the above inequality. Further, we need to now linearize (12a) in the bases of (12) to obtain the stability condition for the flocking state. The full linearization in Fourier space yields the following equation

$$\frac{d}{dt} \begin{pmatrix} \delta \bar{\rho} \\ \delta \bar{\theta} \end{pmatrix} = \begin{pmatrix} -q^2 \xi_t \chi_t \rho^* & -v_{\text{tr}}[\rho^*] \\ -\frac{q^2}{2} B[\rho^*] & 0 \end{pmatrix} \begin{pmatrix} \delta \bar{\rho} \\ \delta \bar{\theta} \end{pmatrix} \quad (15)$$

Here  $B[\rho^*] = (2\xi_0 \chi_t + \xi_r \chi_r) \rho^* - v_s$ . The dispersion relation for  $\omega(q)$  then reads

$$\omega = \frac{i q^2 \xi_r \chi_t \rho^*}{2} \left[ 1 \pm \sqrt{1 + \frac{2 v_{\text{tr}} q^2 B}{q^4 \xi_t^2 \chi_t^2 \rho^{*2}}} \right] \quad (16)$$

with the condition for long-wavelength instability given by:

$$2\xi_0^2 \rho^{*2} \chi_t^2 - \xi_0 \rho^* (2v_s - \xi_r \chi_r \rho^*) \chi_t - v_s (\xi_r \chi_r \rho^* - v_s) > 0$$

Using the above, we can solve for  $\chi_t$ . The solution is:

$$\chi_t^* = \frac{v_s - \frac{\xi_r \chi_r \rho^*}{2}}{2\xi_0 \rho^*} \left[ 1 \pm \sqrt{1 - \frac{2(\xi_r \chi_r \rho^* - 1)}{v_s (1 - \frac{\xi_r \chi_r \rho^*}{2v_s})^2}} \right] \quad (17)$$

Let us consider the negative solution, thus  $\chi_t < \chi_t^*$ . Let us further study the limit  $\frac{\chi_r}{v_s} \ll 1$  (this is justified, since in simulations this value is at most  $\approx 0.2$  - see Table in Appendix. Using the definitions for  $l_r$  and  $l_t$ , the desired inequality is thus

$$l_r^* \gtrsim \frac{2b}{\xi_r} \frac{1}{\rho^*} + \frac{2.73\xi_0 b^3}{\xi_r} l_t \quad (18)$$

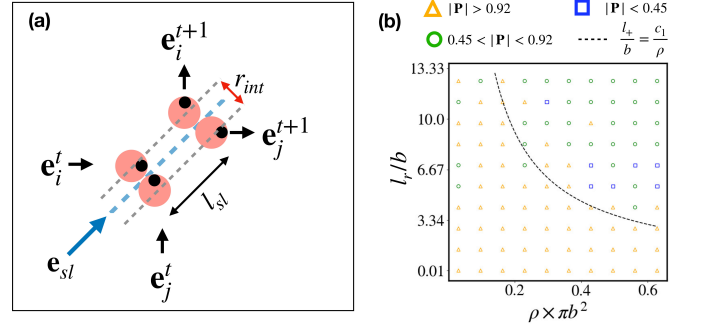


FIG. 5. (a) Schematic of the agent-based-sliding model. (b) phase diagram in the plane of  $(\rho, l_r)$  from the simulations of the agent-based model (to be compared with Fig. 1(a)). Symbols represent steady-state polarization (as opposed to spatial structure) as indicated in the legend. Parameters used are  $v_s = 5$ ,  $c_1 = 0.14$ ,  $r_{int} = 2$ ,  $\frac{1}{\xi} = 30$ , with  $l_t = 0$ .

We can identify this to have the same functional form as Eq.(5) defining the transition line. Equating with Eq. 4 in the main text, we have that

$$c_1 = \frac{2}{\xi_r}, \quad \beta_1 = \frac{2.73\xi_0 b^3}{\xi_r} \quad (19)$$

We can thus infer the values of  $\xi_r \approx 2c_1 \approx 0.028$  and  $\xi_0 \approx 0.122$ . We thus conclude that the noiseless limit of a minimal hydrodynamic model captures the destabilization transition of the flock. In addition, such transitions within between crystalline/disorder phases (e.g. Fig. 3(b)) are also captured, although there is no explicit spatial-structure instability encoded in the hydrodynamic model (e.g. for instance in [37]).

## V. AGENT-BASED-SLIDING MODEL

To further substantiate our findings, we now construct an agent-based model of pair colloids that interact via a sliding-whilst-rotating mechanism. To make progress, we consider the dynamics (1) in the limit of  $e_{x_i} = e_{x_j}$  and  $e_{y_i} = -e_{y_j}$ . This corresponds to any arbitrary incoming collision in the frame of  $\hat{\mathbf{e}}_{sl}$ , as depicted in Fig. 5(a) (the angle  $\theta$  now is strictly speaking deviations from the half angle  $\bar{\theta} = \frac{1}{2}(\theta_i + \theta_j)$ ). In the sliding picture, the 4 degrees of freedom in (1) reduce to 2, for the center of mass motion  $l_{sl}$  and the  $i$ th angle  $\theta_i$  (we could have equivalently considered the relative angle  $\Delta\theta = \theta_i - \theta_j$ , and then reset  $\theta_i = \frac{\Delta\theta}{2}$ ). The evolution of the latter is given by  $\dot{\theta}_i = v_s \cos \theta_i / 4l_{sl}$ , with its solution given by  $\frac{\theta_i}{2} = \tan^{-1} \left( A \exp \frac{tv_s}{4l_{sl}} \right) - \frac{\pi}{4}$ , with  $A = \tan(\frac{\theta_i^0}{2} + \frac{\pi}{4})$  (superscript 0 denoting the incident angle). This solution we see to be idealized since it asymptotes to  $\frac{\pi}{2}$  in the long time limit. We nevertheless see that the outgoing angle grows inversely with  $l_{sl}$ .

To run simulations in our agent-based model, we denote  $\theta_i^0$  ( $\theta_i^f$ ) as the incident (final) angle of agent  $i$  upon collision. Upon interacting with agent  $j$  within an interaction radius  $r_{int}$ , the update equations for the model are such that whilst  $\|\mathbf{r}_i - \mathbf{r}_j\| < r_{int}$

$$\mathbf{r}_i^{t+1} \rightarrow \mathbf{r}_i^t + l_{sl} \mathbf{e}_{sl}, \quad \mathbf{e}_{sl} = \frac{1}{2}(\mathbf{e}_i + \mathbf{e}_j) \quad (20a)$$

$$\theta_i^{t+1} \rightarrow \left(1 - \frac{p_{sl}}{2}\right) \theta_j^t + \frac{p_{sl}}{2} \theta_i^t \quad (20b)$$

with  $j \leftrightarrow i$  for the  $j$ th agent update ( $i$  and  $j$  are updated simultaneously, see schematic in Fig. 5(a)). We assign the probability  $p_{sl}$  of a particular slide of length  $l_{sl}$  as:

$$p_{sl}(l_{sl}) = 1 - \operatorname{erf} \left[ \frac{l_{sl}}{\xi} \left(1 - \frac{l_{sl}^*}{l_{sl}}\right) \right], \quad l_{sl}^* = \frac{r_{int}^2}{4l_+} \quad (21)$$

We note that only pair collisions are considered, whilst outside  $r_{int}$ , the dynamics are simply  $\dot{\mathbf{r}} = v_s \mathbf{e}$  (noiseless self-propelled particles). As it stands, (20) does not resolve individual time steps during the collision, but consists of discrete updates during a collision event.  $p_{sl}$  is constructed such that sufficiently small slides ( $l_{sl} \ll \frac{r_{int}^2}{4l_+}$ ) are more likely hence  $p_{sl} \rightarrow 1$  in the limit of  $\xi \ll 1$  (fully elastic collision, e.g. at high densities). If instead  $l_{sl} \gg \frac{r_{int}^2}{4l_+}$  we have an *aligning collision* with  $\theta_i^f = \frac{1}{2}(\theta_j^0 + \theta_i^0)$ . We note that the other extreme of  $l_r < l_-$  is not considered here; since our aim is to reproduce main features of our chemical interaction-based numerical simulations. We note that the model has thus only one free parameter,  $\xi$ , in addition to the previously defined ones. The results of the simulation are shown in Fig. 5(b), where we see that the phase diagram of Fig. 1 is roughly reproduced. The key difference viz-a-viz Fig. 1 is that in most cases a net polarization is produced, with the delimiting lines of Eq. (5) giving solutions that are fully polarized.

## VI. CONCLUSIONS

To conclude, we present a novel mechanism for formation of fluid flocks that only requires long-ranged (net) repulsive torques and short-ranged repulsive forces from steric interactions. We have shown that this is equivalently abstracted to a sliding-whilst-rotating mechanism at the pair colloidal level. Although the roles of excluded volume interactions [15, 16, 19, 21], repulsive torques - either short [15] or long [26] ranged - and long-ranged repulsive forces [21, 26] have been studied separately, we have analyzed here the individual contributions of each of those components, and argued that the former two are the minimal requisite components. Our mechanism can be summarized as follows: the pair colloids slide together for at least a unit length before deterministically rotating away from each other. This is required to break the forward-backward symmetry at the pair-collision level. Destabilizing of the flock arises due to

symmetric collisions at the pair colloidal level, wherein they slide exceedingly short before rotating away upon collision. These results we show to be consistent with a coarse-grained hydrodynamic theory, though the transition lines are greatly overestimated wherein, indicating the need to go beyond conventional coarse-graining hypotheses [16, 17]. We then use this sliding-whilst-rotating mechanism as a basis for a phenomenological agent-based model based on update rules of colliding pair colloids, where we further find that it reproduces our results well with only one additional free parameter; further substantiating the underlying fluid flock forming mechanism.

The CLF (or the polar liquids) are both generated by, and further destabilized by, the deterministic torques themselves. Notably, the apparent ubiquitous role of noise in destabilizing flocks [4, 11, 21, 26] is also absent in our mechanism (these are negligibly small in our simulation). We note that in the absence of short-ranged excluded volume repulsions, our results would converge to that recently studied in [26] where the need for (long-ranged) repulsive forces is more imminent. Translational repulsion merely renders the flock to acquire a crystalline structure. We also have not studied here the role of particle shape anisotropy [14, 17], which would add additional competing length scales to our analysis. Finally, the agent-based model presented here being minimal, and still does not account for the crystalline flock for  $l_t > 0$  (due to purely local interaction rules), which suggests extensions for future work. We expect our results here to be directly relevant to a variety of experimental systems. For example, migrating cell collections have been widely reported to exhibit spatial organization resembling a polar fluid [22, 28], while their interaction mechanism has been known to include (among others) long-ranged chemotaxis and avoidance torques [27]. The presented mechanism being very generic, we expect it to also be relevant for interacting colloids of non-chemical origin [25, 37, 38], where the underlying mechanism should also hold.

## ACKNOWLEDGMENTS

We thank Professor Mike Cates for discussions. AGS acknowledges funding from the DIA Fellowship from the Government of India. SA acknowledges support from the National Postdoctoral Fellowship (SERB File number: PDF/2023/002096) provided by ANRF, Government of India. RS acknowledges support from seed and initiation grants from IIT Madras as well as a Start-up Research Grant from SERB (SERB File Number: SRG/2022/000682), India.

FIG	$L$	$dt$	$b$	$v_s$	$\kappa$	$N$	$\chi_t$	$\chi_r$	$D_r$	$D_t$
1	100	0.01	1	50	175	(319, 2578)	0	(0, 7)	$10^{-6}$	$10^{-8}$
3.(a)	100	0.01	1	50	175	1024	(0, 5)	(0, 10)	$10^{-6}$	$10^{-8}$
3.(b)	100	0.01	1	50	175	1024	(-1, 0)	(0, 10)	$10^{-6}$	$10^{-8}$
3.(d)	186	0.01	1	50	175	4000	0	0.75	$10^{-6}$	$10^{-8}$
3.(e)	186	0.01	1	50	175	4000	3	6	$10^{-6}$	$10^{-8}$
4.(a)	(77, 354)	0.01	1	50	175	1600	0	(0, 9)	$10^{-6}$	$10^{-8}$
4.(b)	118	0.01	1	50	175	1600	(0, 12)	(0, 32)	$10^{-6}$	$10^{-8}$
5.(b)	100	0.1	NA	5	NA	(319, 2578)	0	(0, 15)	NA	NA

TABLE I. Parameter values used for respective figures in the main text. Note that we consider noise to be less dominant to deterministic effects. Indeed, for the results in this paper, the Péclet number  $Pe = v_s/(bD_r)$  is around  $10^9$ .

## APPENDIX

### Appendix A: Simulation details

The update equations is given in Eq. 1 of the main text. The position and orientations of the particles are updated using a forward Euler-Maruyama method. Initially particles are distributed randomly over the two-dimensional space. The initial orientations are also randomly distributed over the range of angles  $[-\pi, +\pi]$  (angles are computed with respect to the positive  $x$ -axis). Periodic boundary conditions are applied on both the  $x$ -axis and  $y$ -axis. To compute chemical interactions using the expression of  $\mathbf{J}_i$ , we need to sum over periodic images. We have used a regular summation convention (using minimum image convention) for all results reported here, and checked these with the full Ewald summation convention for selected parameter values. The parameter values used are given here: radius of a colloid  $b = 1$ , velocity  $v_s = 50$ , total number of particles  $N$  is variable according to the figure. All simulations are performed using periodic boundary conditions with a regular summation convention. A summary of all of these is given in the Table (I). For the agent-based model (Fig.5), additional parameters used are mentioned in the caption of Fig.5.

### Appendix B: Correlation functions and fluctuations

The pair distribution function  $g(r, \phi, \theta)$  implies correlations and provides the probability density of finding a pair of particles at a distance  $r$  with relative angles  $\phi$  and  $\theta$ . The angle  $\phi$  is between the relative position  $r$  and the self-propulsion direction of the tagged particle,  $\hat{\mathbf{e}}_i \cdot \hat{\mathbf{r}}_{ij} = \cos \phi$  and  $\theta$  is the angle between the propulsion directions of the particle pair. To obtain this pair distribution function, histograms are created with the number of particles  $N_h(r, \phi, \theta)$  at distance  $r$ , positional angle  $\phi$  and relative angle  $\theta$ . The bins are chosen as  $0.1b$  for  $r$ ,  $\pi/150$  for  $\phi$  and  $\pi/2$  for  $\theta$ . Then we need to normalize  $N_h(r, \phi, \theta)$ , to obtain the pair distribution function  $g(r, \phi, \theta)$ . The number of configurations is

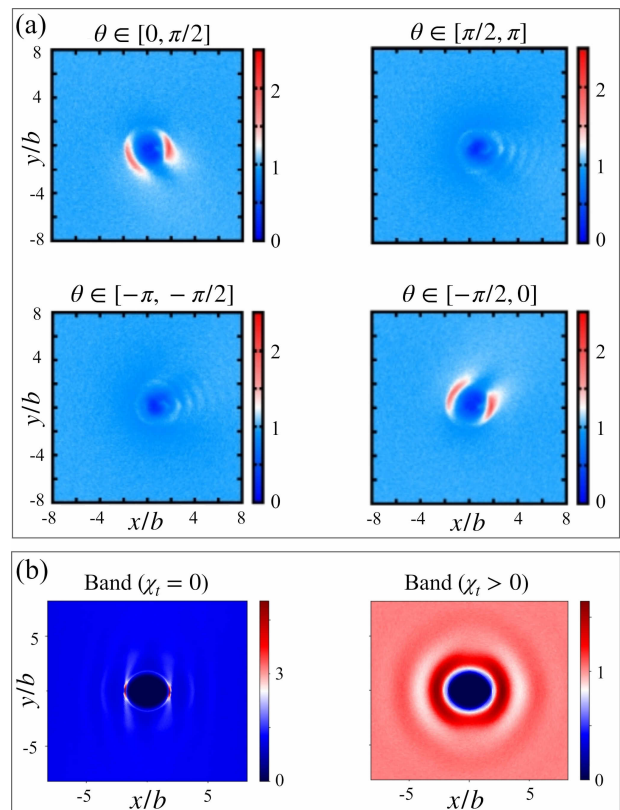


FIG. 6. Pair correlation function  $g(r, \phi, \theta)$  for the isotropic phase for four different  $\theta$  ranges in panel (a). Pair correlation function  $g(r, \phi)$  in the band phase for  $\chi_t = 0$  and  $\chi_t > 0$  in (b).

$t_c$  (10000 snapshots), over which histograms are made. The area of the annular segment of radial width  $dr$ , angular width  $d\phi$  is given by  $A_r = r dr d\phi$ . The number density is  $\rho = N/L^2$  and the size of the relative orientation bin is  $d\theta$ . Then the normalization factor is  $N_r = \frac{A_r \rho N t_c d\theta}{2\pi}$  and the pair distribution function is given by  $g(r, \phi, \theta) = N_h(r, \phi, \theta)/N_r$ .

An example of this for isotropic phase is given in Fig. 6(a). The pair distribution functions are determined

for the four different  $\theta$  ranges as:  $\theta:[0, \pi/2]$ ,  $\theta:[\pi/2, \pi]$ ,  $\theta:[-\pi, -\pi/2]$  and  $\theta:[-\pi/2, 0]$ . We see that in the isotropic phase, the probability of finding a neighboring particle is different in the front relative to the back of the direction of motion (orientation), indicative of the symmetry breaking in an active disordered gas [17, 26, 38]. In the main text, we show that  $g(r, \phi)$  also distinguishes CLFs from CCFs, the former having a more quadrant-like structure compared to the latter's hexatic structure. In addition, we compare the structure of  $g(r, \phi)$  for the band phases in Fig. (6)(b), for the CLF and CCF density bands. Note that the band structure is more dense in the case of  $\chi_t = 0$ , resulting a more intense correlation in  $g(r, \phi)$ . A related quantity that we compute is the radial  $g(r)$ , given by

$$g(r) = \frac{1}{N} \sum_{i,j} \langle \delta(|\mathbf{r}_i - \mathbf{r}_j| - r) \rangle \quad (\text{B1})$$

this is plotted in Fig. (3)(f), distinguishing the CLF and CCF.

To further compare the CLF and CCF, we measure the following quantities.

### 1. Velocity correlations

We define the velocity correlation as

$$C_v(r) = \langle \mathbf{e}_i \mathbf{e}_j \rangle_{|\mathbf{r}_i - \mathbf{r}_j| = r}$$

The above is plotted for the two cases of CLF and CCF in Fig.7.

### 2. Orientational (angular) fluctuations

This is given by  $\langle (\Delta\theta)^2 \rangle = \langle \theta^2 \rangle - \langle \theta \rangle^2$ . Here,  $\langle \rangle$  denotes average over colloids. See Fig.(8).

### 3. Giant number fluctuations.

This is given  $\langle (\Delta N)^2 \rangle = \langle N^2 \rangle - \langle N \rangle^2$  where  $N$  is the number of particles found in a given box size (the grid is binned into boxes). Here,  $\langle \rangle$  is performed over bins. See Fig.(8).

### Appendix C: Description of the supplementary movies

The time evolution of the CCF and CLF structures for a larger system with total number of particles  $N = 20000$ , are attached as supplementary movies [29]. We note that our results are robust as we change number of particles in the simulations. For both cases, we started with random

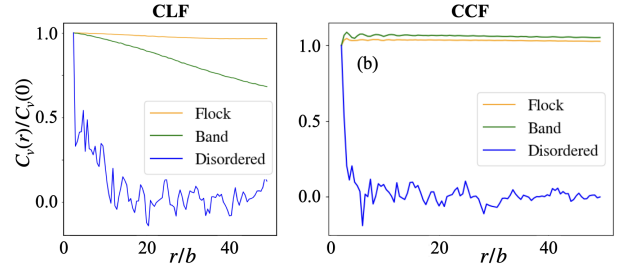


FIG. 7. Velocity correlations for the CLF (left) and CCF (right). In both cases, the disordered gas shows exponential decay to zero at large distances. In the flocking case, both are unity across long distances (globally polarized). In the band phase (green), the correlations in the CLF decay whereas those in the CCF do not.

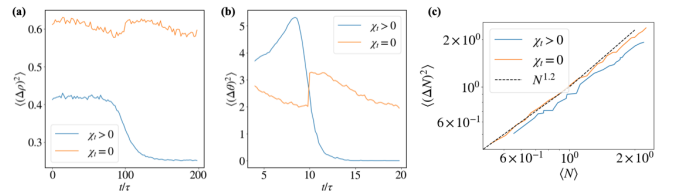


FIG. 8. Comparison of CLF and CCF via (a) density fluctuations, (b) orientational fluctuations, and (c) giant number fluctuations. For the CLF, (a) shows residual fluctuations, whereas for the CCF, the fluctuations die out in the steady-state. In (b), a similar phenomenon is seen for the orientational fluctuations. Note that both curves are strongly correlated (shared monotonicity). In (c) the giant number fluctuations of both show an enhanced exponent  $\sim 1.2$ .

initial conditions (positions and orientations), and update the equation of motion following Eq. 1. In both movies, the particles are colored by their orientations (given in terms of the angle  $\theta$  their orientation vector makes with the positive  $x$ -axis). The color bar is same as the one used in Fig. 1. Two particles are intentionally colored black throughout the simulation to simply trace them during the dynamics. Polar order or the flocking state collectively emerges in this model with both the cases. Parameters used for the two movies are below.

- **Movie I.** In the case of  $\chi_t = 0$  (CLF), the liquid flock gradually forms throughout the system and moves in a particular direction. The fixed parameter values are:  $L = 418$ ,  $b = 1$ ,  $dt = 0.01$ ,  $D_r = 10^{-3}$ ,  $D_t = 10^{-3}$ ,  $\kappa = 175$ ,  $v_s = 50$ ,  $\chi_t = 0$ ,  $\chi_r = 0.75$ .
- **Movie II.** In the case of  $\chi_t > 0$  (CCF), the particles first start to form local polar flocks (colored patch), then merge and pick a particular direction of motion entirely. The fixed parameter values are:  $L = 418$ ,  $b = 1$ ,  $dt = 0.01$ ,  $D_r = 10^{-3}$ ,  $D_t = 10^{-3}$ ,  $\kappa = 175$ ,  $v_s = 50$ ,  $\chi_t = 3$ ,  $\chi_r = 6$ .

- [1] J. Toner, *The Physics of Flocking: Birth, Death, and Flight in Active Matter* (Cambridge University Press, 2024).
- [2] I. D. Couzin, J. Krause, R. James, G. D. Ruxton, and N. R. Franks, Collective memory and spatial sorting in animal groups, *Journal of theoretical biology* **218**, 1 (2002).
- [3] T. Vicsek, A. Czirók, E. Ben-Jacob, I. Cohen, and O. Shochet, Novel type of phase transition in a system of self-driven particles, *Physical review letters* **75**, 1226 (1995).
- [4] H. Chaté, F. Ginelli, G. Grégoire, and F. Raynaud, Collective motion of self-propelled particles interacting without cohesion, *Physical Review E—Statistical, Nonlinear, and Soft Matter Physics* **77**, 046113 (2008).
- [5] J. Toner, Y. Tu, and S. Ramaswamy, Hydrodynamics and phases of flocks, *Annals of Physics* **318**, 170 (2005).
- [6] J. Toner, Birth, death, and horizontal flight: Malthusian flocks with an easy plane in three dimensions, *Phys. Rev. E* **110**, 064604 (2024).
- [7] A. Maitra, P. Jentsch, L. Chen, C. F. Lee, J. Toner, and S. Ramaswamy, The inconvenient truth about flocks, arXiv preprint arXiv:2503.17064 (2025).
- [8] H. Ikeda, Minimum scaling model and exact exponents for the nambu-goldstone modes in the vicsek model, *Physical Review Letters* **133**, 258301 (2024).
- [9] H. Chaté and A. Solon, Dynamic scaling of two-dimensional polar flocks, *Physical Review Letters* **132**, 268302 (2024).
- [10] P. Jentsch and C. F. Lee, New universality class describes vicsek’s flocking phase in physical dimensions, *Physical Review Letters* **133**, 128301 (2024).
- [11] S. Adhikary and S. Santra, Pattern formation and phase transition in the collective dynamics of a binary mixture of polar self-propelled particles, *Physical Review E* **105**, 064612 (2022).
- [12] S. Adhikary and S. Santra, Collective dynamics and phase transition of active matter in presence of orientation adapters, arXiv preprint arXiv:2302.13035 (2023).
- [13] M. E. Cates and C. Nardini, Active phase separation: new phenomenology from non-equilibrium physics, *Reports on Progress in Physics* **88**, 056601 (2025).
- [14] H. Wensink and H. Löwen, Emergent states in dense systems of active rods: from swarming to turbulence, *Journal of Physics: Condensed Matter* **24**, 464130 (2012).
- [15] M. Knežević, T. Welker, and H. Stark, Collective motion of active particles exhibiting non-reciprocal orientational interactions, *Scientific Reports* **12**, 19437 (2022).
- [16] L. Chen, K. J. Welch, P. Leishangthem, D. Ghosh, B. Zhang, T.-P. Sun, J. Klukas, Z. Tu, X. Cheng, and X. Xu, Molecular chaos in dense active systems, arXiv preprint arXiv:2302.10525 (2023).
- [17] R. Großmann, I. S. Aranson, and F. Peruani, A particle-field approach bridges phase separation and collective motion in active matter, *Nature communications* **11**, 5365 (2020).
- [18] J. Chen, X. Lei, Y. Xiang, M. Duan, X. Peng, and H. Zhang, Emergent chirality and hyperuniformity in an active mixture with nonreciprocal interactions, *Physical Review Letters* **132**, 118301 (2024).
- [19] A. Martín-Gómez, D. Levis, A. Díaz-Guilera, and I. Pagonabarraga, Collective motion of active brownian particles with polar alignment, *Soft matter* **14**, 2610 (2018).
- [20] E. Sese-Sansa, I. Pagonabarraga, and D. Levis, Velocity alignment promotes motility-induced phase separation, *Europhysics Letters* **124**, 30004 (2018).
- [21] L. Caprini and H. Löwen, Flocking without alignment interactions in attractive active brownian particles, *Physical Review Letters* **130**, 148202 (2023).
- [22] T. Hiraiwa, Dynamic self-organization of idealized migrating cells by contact communication, *Physical Review Letters* **125**, 268104 (2020).
- [23] M. Kumar, A. Murali, A. G. Subramaniam, R. Singh, and S. Thutupalli, Emergent dynamics due to chemohydrodynamic self-interactions in active polymers, *Nature Commun.* **15**, 4903 (2024).
- [24] A. G. Subramaniam, M. Kumar, S. Thutupalli, and R. Singh, Rigid flocks, undulatory gaits, and chiral foldamers in a chemically active polymer, *New Journal of Physics* **26**, 083009 (2024).
- [25] A. Bricard, J.-B. Caussin, N. Desreumaux, O. Dauchot, and D. Bartolo, Emergence of macroscopic directed motion in populations of motile colloids, *Nature* **503**, 95 (2013).
- [26] S. Das, M. Ciarchi, Z. Zhou, J. Yan, J. Zhang, and R. Alert, Flocking by turning away, *Physical Review X* **14**, 031008 (2024).
- [27] B. A. Camley and W.-J. Rappel, Physical models of collective cell motility: from cell to tissue, *Journal of physics D: Applied physics* **50**, 113002 (2017).
- [28] M. Hayakawa, T. Hiraiwa, Y. Wada, H. Kuwayama, and T. Shibata, Polar pattern formation induced by contact following locomotion in a multicellular system, *Elife* **9**, e53609 (2020).
- [29] See the supplemental material at this url: .
- [30] S. Saha, R. Golestanian, and S. Ramaswamy, Clusters, asters, and collective oscillations in chemotactic colloids, *Phys. Rev. E* **89**, 062316 (2014).
- [31] R. Soto and R. Golestanian, Self-assembly of active colloidal molecules with dynamic function, *Phys. Rev. E* **91**, 052304 (2015).
- [32] G. Rückner and R. Kapral, Chemically powered nanodimers, *Physical review letters* **98**, 150603 (2007).
- [33] R. Singh, R. Adhikari, and M. Cates, Competing chemical and hydrodynamic interactions in autophoretic colloidal suspensions, *The Journal of chemical physics* **151** (2019).
- [34] Indeed, the polar order is expected to be destroyed at larger values of fluctuations [3]. In this paper, we choose noise to be less dominant to deterministic effects by choosing Péclet number  $Pe = v_s/(bD_r)$  to be around  $10^9$ .
- [35] B. V. Hokmabad, J. Agudo-Canalejo, S. Saha, R. Golestanian, and C. C. Maass, Chemotactic self-caging in active emulsions, *Proc. Natl. Acad. Sci.* **119**, e2122269119 (2022).
- [36] D. Geyer, A. Morin, and D. Bartolo, Sounds and hydrodynamics of polar active fluids, *Nature materials* **17**, 789 (2018).
- [37] D. Geyer, D. Martin, J. Tailleur, and D. Bartolo, Freezing a flock: Motility-induced phase separation in polar active liquids, *Physical Review X* **9**, 031043 (2019).
- [38] J. Zhang, R. Alert, J. Yan, N. S. Wingreen, and

- S. Granick, Active phase separation by turning towards regions of higher density, *Nature Physics* **17**, 961 (2021).
- [39] R. A. Simha and S. Ramaswamy, Statistical hydrodynamics of ordered suspensions of self-propelled particles: waves, giant number fluctuations and instabilities, *Physica A: Statistical Mechanics and its Applications* **306**, 262 (2002).
- [40] J. Deseigne, S. Léonard, O. Dauchot, and H. Chaté, Vibrated polar disks: spontaneous motion, binary collisions, and collective dynamics, *Soft Matter* **8**, 5629 (2012).
- [41] P. M. Chaikin, T. C. Lubensky, and T. A. Witten, *Principles of condensed matter physics*, Vol. 10 (Cambridge university press Cambridge, 1995).